ACS OMEGA

Open Access

http://pubs.acs.org/journal/acsodf

Article

Sensitive Aluminum SPR Sensors Prepared by Thermal Evaporation Deposition

Chengchao He,[†] Yanhong Li,[†] Yuxiang Yang, Huaikun Fan, Dawei Li, and Xue Han*

Cite This: *ACS Omega* 2023, 8, 43188−43196

Read Online

ACCESS | Metrics & More | Article Recommendations | Supporting Information

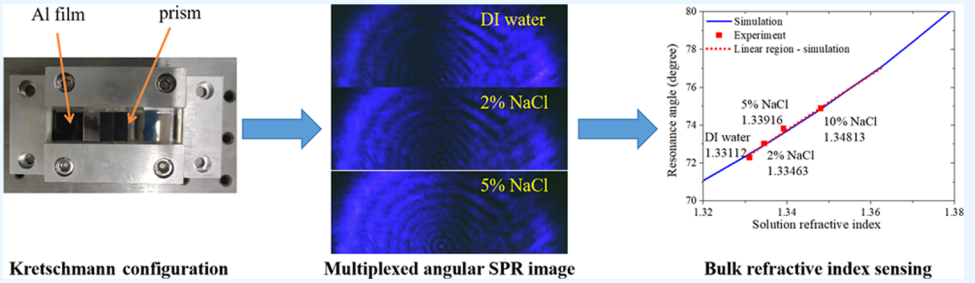

ABSTRACT: We used straightforward thermal evaporation deposition to form thin Al films on fused silica slides as surface plasmon resonance (SPR) sensors in the blue visible region. Compared to other studies, we achieved high-quality Al SPR sensors with a low vacuum level at 7×10^{-4} Pa and a low deposition rate between 1.47 and 3.41 nm/s. These Al films have an atomic-level surface roughness. With our recipe, the requirements for deposition conditions are relaxed, and the operation time is reduced remarkably. The experimental sensitivity of the bulk refractive index measurements using 405 nm probing light is as high as 149.9°/RIU. Compared with other studies, our blue visible Al SPR completes the Al SPR working frequency range from deep UV to near-infrared which is much broader than the working range of Au SPR sensors. The cost of Al material is cheap, and the deposition instrument is also economic and operation easy. Considering the compatibility with most of the nanofabrication procedures and stability from the native oxide layer, Al SPR sensors have a huge potential to replace Au SPR sensors as the new golden standard of SPR sensing technology.

INTRODUCTION

Sensing technology based on the propagation surface plasmon resonance (SPR) phenomenon has been developed for more than 40 years since its first application in gas sensing in the early 1980s.[1] It has been developed prosperously.[2−4] Noble metals, e.g., Au and Ag, are the most used metallic materials for SPR sensors.[5−7] Chemical instability prohibits Ag SPR sensor applications in aqueous or humid environments. Although Au SPR sensors are the gold standard in the industry, there are limitations to these sensors. A few nanometers of a Cr layer is utilized to improve the adhesion of the Au layer due to its high dewetting effect. The extra Cr layer prevents a Au SPR chip from reaching the optimum sensing performance. Au only supports SPR in a short range of wavelengths in the red visible and near-infrared, and it cannot work in the blue visible or UV regimes due to the interband transition. Cost is another factor that motivates researchers to study other materials for SPR sensors. Pursuing SPR resonance beyond the visible regime is another hot research topic since various light−matter interactions and nonlinear optical phenomena can be excited simultaneously for multichannel transduction sensing.[8−10]

Al is a competitive candidate due to its low cost, long SPR resonance range (deep UV to near-infrared), stability due to the native oxide layer, and compatibility with complementary metal−oxide−semiconductor (CMOS) fabrication processes. Many research works studied the localized SPR (LSPR) properties of Al nanostructures.[11,12] These Al nanostructures are outperforming, especially in the deep UV regime.[13−15] Regarding the propagation SPR based on Al thin films, a few research works have shown that Al has superior SPR sensing performance in UV and deep UV,[16] visible red,[17] and near-infrared regimes.[18]

In this work, we used a simple thermal evaporation deposition technique to deposit Al thin films. We examined the effects of different vacuum levels and deposition rates on the quality of Al thin films, i.e., the complex refractive index. We conducted bulk and surface sensing experiments to demonstrate the SPR performance of the deposited Al thin films. We achieved as high as 149.9°/RIU sensitivity using a homemade multiplexed angular interrogation system at 405

Received: September 8, 2023
Revised: October 10, 2023
Accepted: October 17, 2023
Published: November 2, 2023

nm for the first time. To the best of our knowledge, this value is the highest among metallic film-based SPR sensors. This work demonstrates that simple, economic thermal evaporation deposition can achieve high-quality Al thin films using a low vacuum and a slow deposition rate recipe. Resonance in the blue visible of Al SPR achieved in this work makes it possible to select any frequency from deep UV to the near-infrared to support a specific light−matter interaction or nonlinear optical effect for multichannel transduction sensing. Al SPR sensors are becoming the next generation of the gold standard for SPR sensing techniques.

METHODS

Different deposition technologies are available for Al thin film deposition, e.g., direct current (DC) magnetron sputtering,[19] epitaxial growth,[20,21] electron beam evaporation,[22] and thermal evaporation.[23] Deposition conditions influence the qualities of Al thin films dramatically. We used a thermal evaporator to deposit Al thin films on UV-grade fused silica substrates without heating. Simplicity and low cost are the advantages of this apparatus. Based on the literature, a high chamber vacuum level and a fast deposition rate are mandatory to prevent oxidization by the residue gas during the deposition process to achieve a high-purity Al film.[22,23] We selected two vacuum levels (1×10^{-4} Pa as high and 7×10^{-4} Pa as low) and two heating currents (determine deposition rates) (150 A as high and 120 A as low). We used three deposition conditions, high vacuum + high rate (HH), low vacuum + high rate (LH), and low vacuum + low rate (LL), to examine the Al thin films in terms of optical properties and surface roughness. Details of the deposition procedure are described in the Supporting Information. A few Al films with different thicknesses under the same conditions are tested to check the stability of the deposition.

Regarding the optical property, we used an ellipsometer to measure the real (n) and imaginary (k) parts of the complex refractive indices of the deposited Al films. After the deposition, a native alumina film formed in the room atmosphere. A bilayer model is used to fit the thickness and complex refractive index of the Al layer. The alumina layer is set with different thicknesses (1−4 nm) using the Cauchy model. The Al layer is fitted with the Kramers−Kronig model.[24] Throughout this article, the thicknesses of the aluminum layer and the native alumina layer are indicated separately.

To calibrate the SPR properties, we measured the angular reflectance curves of these Al films in air using a 405 nm laser diode (LD) with a homemade angular interrogation system built on a rotation stage (highest resolution 0.00125°). The Kretschmann configuration provides the wave vector matching condition with a right-angle prism. The probing light is a collimated beam, and the incident angle is scanned over a broad range to cover the entire curve. We compared the experimental and simulated SPR curves for each Al thin film. The n and k of the Al material in COMSOL Multiphysics model are set as the measured values. We examined the resonance angle θ_R, the reflectance at the resonance angle $R(\theta_R)$, and the full width at half-maximum (FWHM) of each SPR curve.

The bulk refractive index sensing capability is studied theoretically to determine the optimized thickness of the Al film for gas (from n = 1 to 1.01) and aqueous (from n = 1.33 to 1.34) cover medium. The thickness of the Al film changes from 10 to 40 nm (excluding native Al_2O_3 thickness) with 1 nm interval, and the incident angle is scanned from 35 to 55° with a 0.05° interval. The n and k of the Al material in the simulation models are the averaged ellipsometry results of different Al films from the same deposition condition. The sensitivity (S) and figure of merit (FOM) are determined using eqs 1 and 2. Here, $\Delta\theta$ is the resonance angle shift, and Δn is the bulk refractive index change of the cover medium.

$$S = \frac{\Delta\theta}{\Delta n} \tag{1}$$

$$\mathrm{FOM} = \frac{S}{\mathrm{FWHM}} \tag{2}$$

Sensing capability of the Al SPR sensors is experimentally tested by measuring NaCl solutions. The refractive indices of these solutions are measured using an Abbe refractometer.[25] The homemade angular interrogation setup is modified (Figure 1a) for a multiplexed angle incidence. An equilateral prism is used in the Kretschmann configuration (Figure 1b). The collimated beam impinges the focusing lens to generate a range of incident angles ($\theta_{final} - \theta_{initial}$ = 5.5296°). Another lens collimates the reflected beam. A CCD images the reflected beam with a resolution of 0.0054°/pixel. The incident angle at the fused silica/Al interface is calculated based on Snell's Law. A black bar is shown at the resonance angle (Figure 1b inset). A polarizer is arranged right after the 405 nm LD to modify the beam intensity. A background image (LD turned off) and a reference image (at the total internal reflection) are collected to calculate the absolute reflectance. The deionized (DI) water

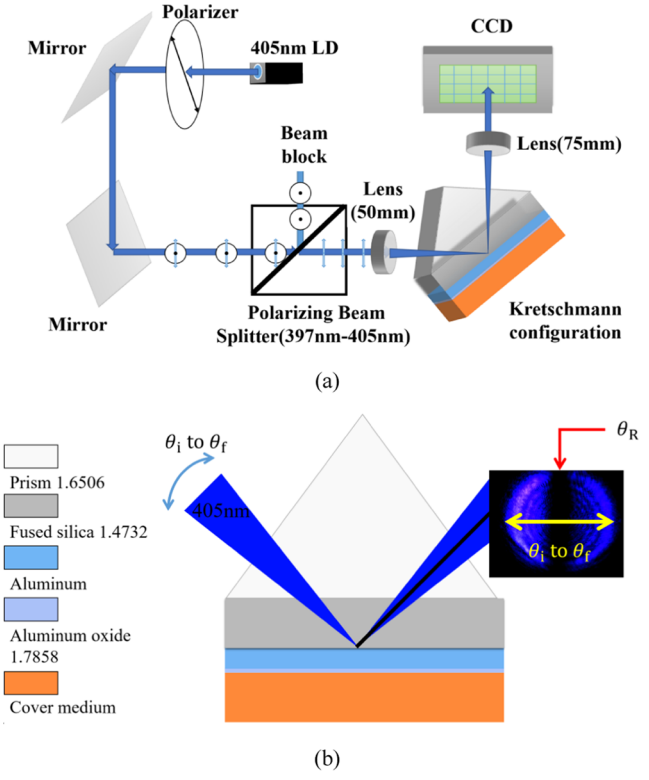

Figure 1. (a) Multiplexed angular interrogation experimental setup. (b) Schematic of the Kretschmann configuration. The refractive index of each layer at 405 nm is presented.

https://doi.org/10.1021/acsomega.3c06855
ACS Omega 2023, 8, 43188−43196

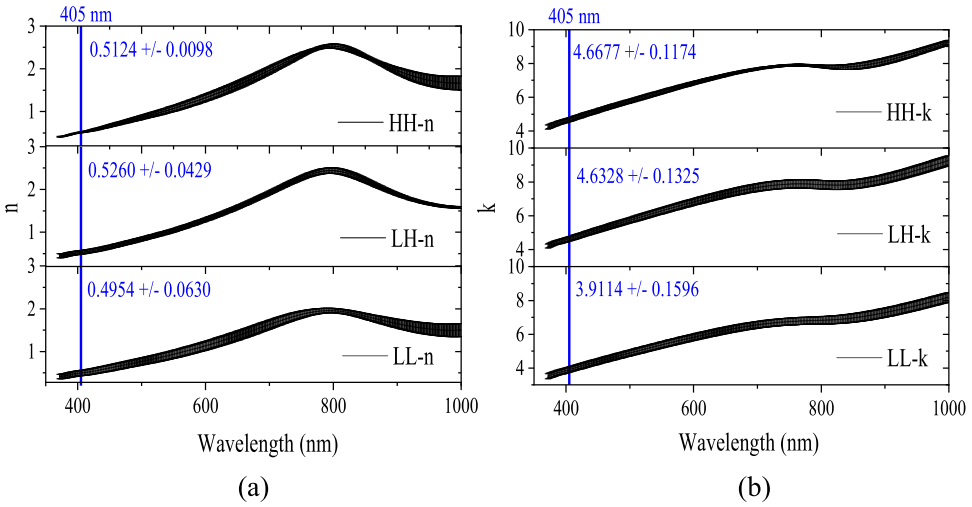

Figure 2. Average (a) real and (b) imaginary refractive indices with standard deviations of Al films deposited by using high vacuum + high rate (HH), low vacuum + high rate (LH), and low vacuum + low rate (LL) conditions.

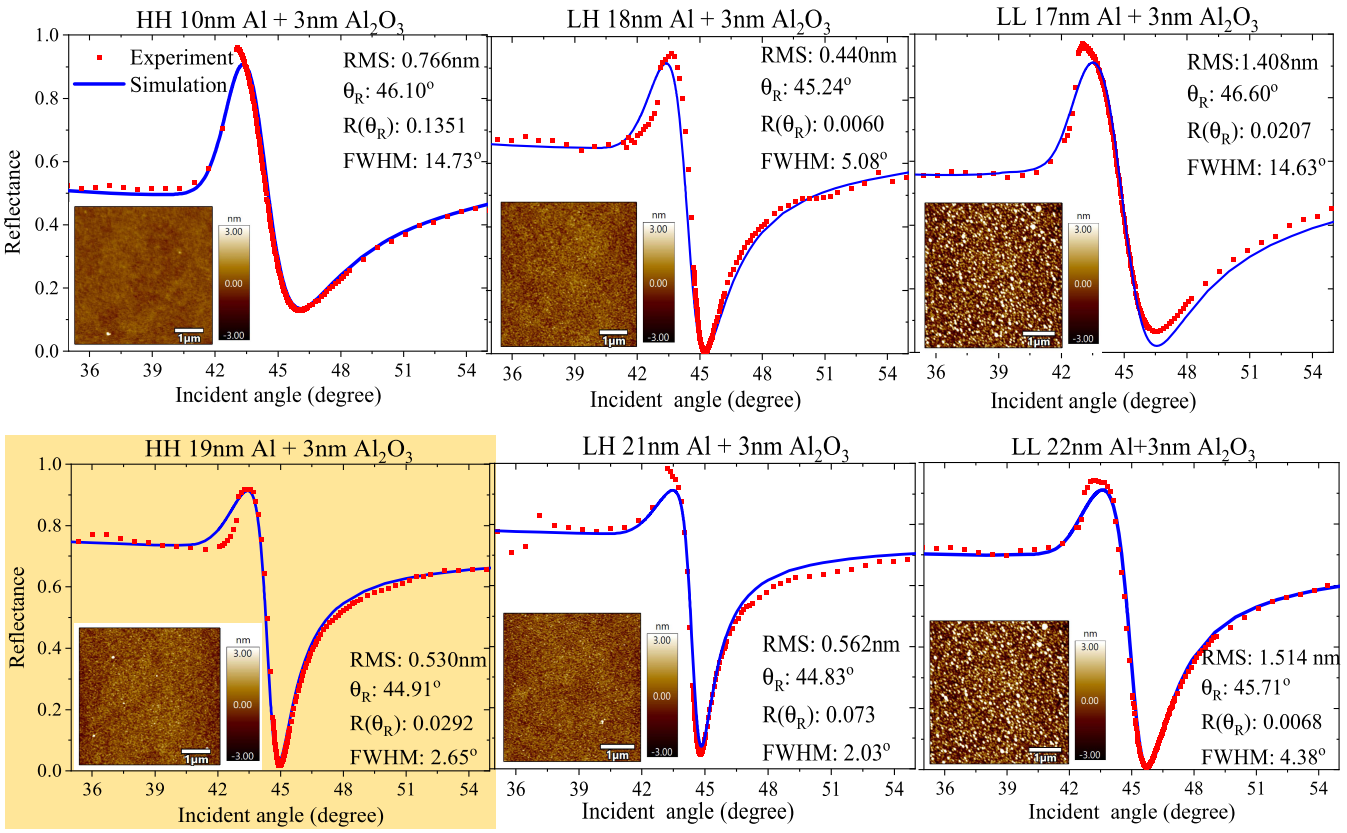

Figure 3. Angular SPR curves of Al films from HH, LH, and LL deposition conditions. Solid blue curve: simulated result; red dotted curve: experimental result. The AFM image of each film is shown as the inset at the left bottom. SPR parameters are calculated based on simulation.

and 2, 5, and 10 wt % NaCl solutions are injected into the flow cell sequentially.

We tested the surface sensing capability of the Al SPR sensor by injecting oxidized cytochrome-c protein solution (7.44 mM) into the flow cell. The resonance angle of the phosphate buffer (0.2 M Na_2HPO_4 + 0.2 M NaH_2PO_4) is measured first. After the protein solution injection, we recorded the angle-multiplexed SPR images at time points 0, 5, and 10 min.

RESULTS

Optical Constants of Deposited Al. Regarding the ellipsometry data fitting, 3 nm alumina provides the lowest mean-squared error (MSE) for most cases (0.6 to 0.8), and the largest MSE is 1.832. The results of 1−4 nm alumina fittings are presented in Supporting Information (Figure S1). We examine the averaged *n* (Figure 2a) and *k* (Figure 2b) of different films from the same deposition condition. The standard deviation demonstrates the stability of the thermal evaporation deposition process. Compared to the other two

https://doi.org/10.1021/acsomega.3c06855
ACS Omega 2023, 8, 43188−43196

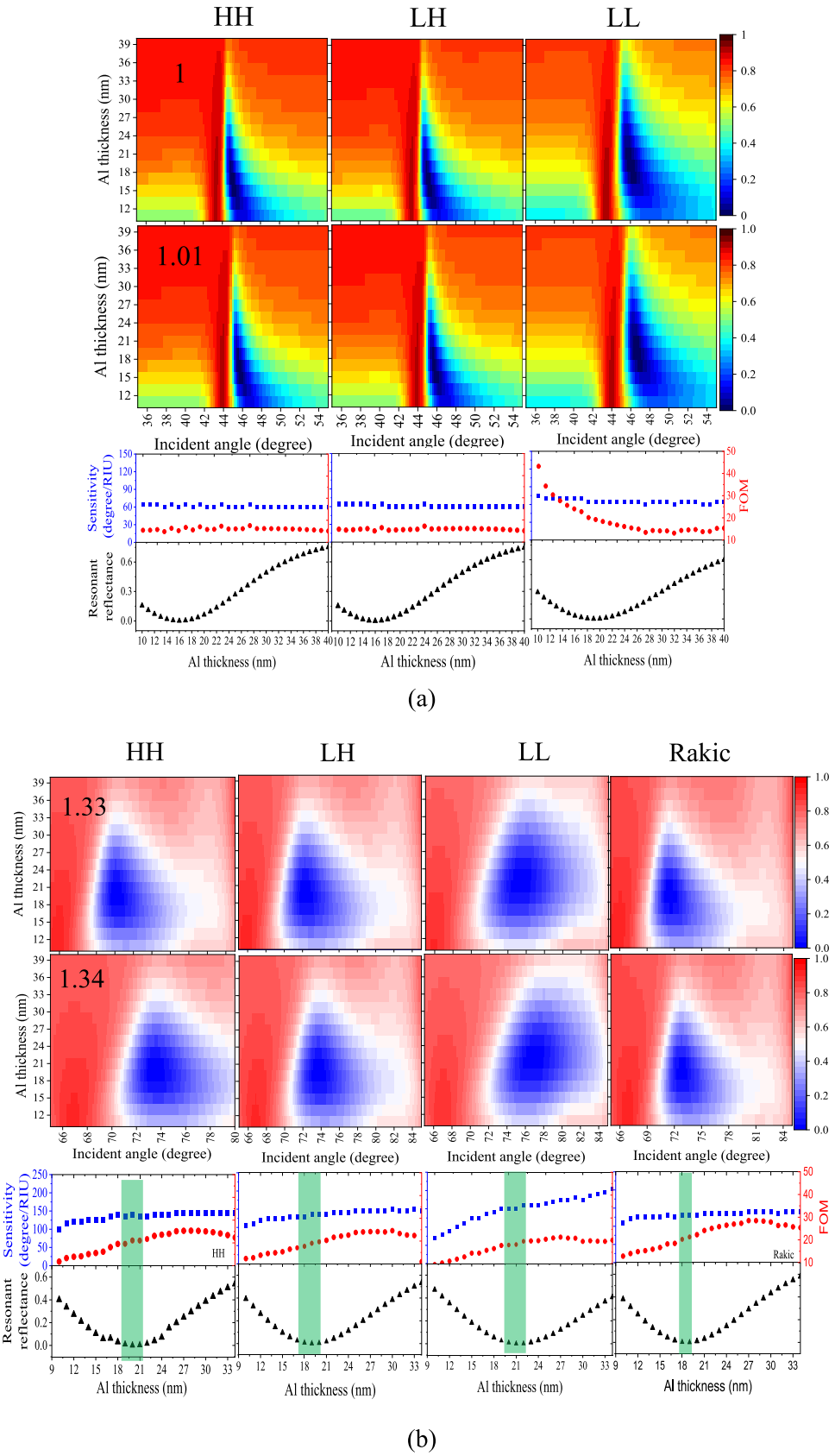

Figure 4. Simulated SPR angular curves as a function of Al film thicknesses. The bulk refractive index change of the cover medium is set (a) from 1 to 1.01 for gas and (b) from 1.33 to 1.34 for aqueous solution sensing. The sensitivity, FOM, and resonant reflectance are shown in the last row.

conditions, Al thin films from the LL condition have lower n and k. The variances are slightly higher, too. For HH and LH conditions, n and k are close to Rakic values[24] (Supporting Information, Figure S2).

https://doi.org/10.1021/acsomega.3c06855
ACS Omega 2023, 8, 43188−43196

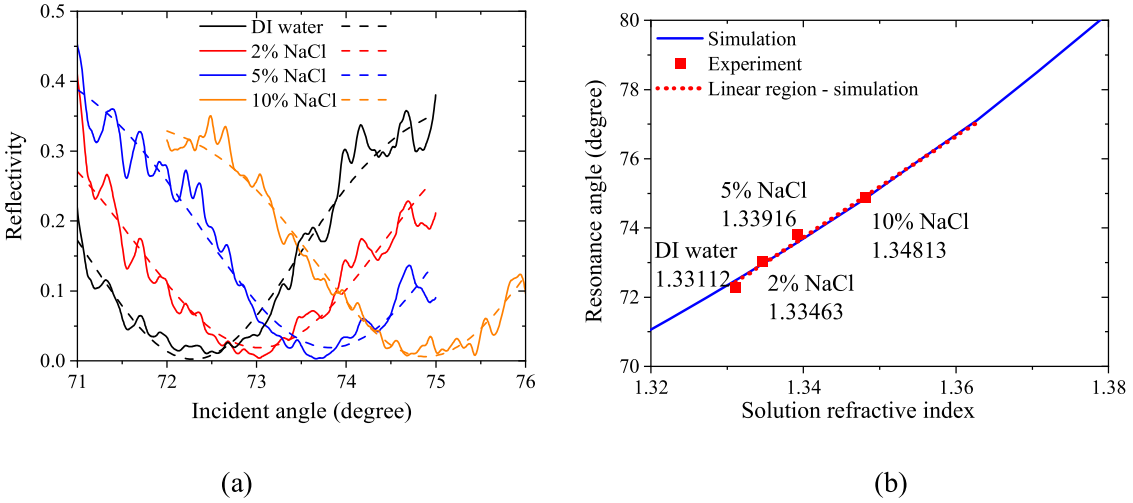

Figure 5. (a) Experimental SPR curves and the fitting curves of 4 different NaCl concentration solutions. (b) SPR resonance angle versus cover medium refractive index. Blue solid curve: simulated result; red square dot: experimental result; red dotted curve: linear transduction regime.

Experimental SPR in Air. The angular SPR curves in air are measured and compared with the simulation results (Figure 3). The experimental result matches the simulation for all of the Al films. We observed that the 19 nm Al film from the HH condition and the 21 nm Al film from the LH condition have the best two SPR curves, i.e., the lowest resonant reflectance and the narrowest FWHM. We should be aware that these two Al films are improper for gas sensing (refractive index around 1) using a 405 nm probing light. As shown in the theoretical result in the following section, the Al films having thicknesses of 16 nm from HH and LH conditions and 19 nm from LL conditions are the most sensitive ones for gas sensing. The atomic force microscopy (AFM) of each film is shown as the inset. For HH and LH conditions, Al thin films have smooth surfaces with atomic-level roughness.[20] The LL condition provides relatively rough Al thin films.

Theoretical Calculation of Bulk Sensitivity and FOM. The deposition condition determines the complex refractive index of Al thin films, and there is an optimum thickness of the Al thin film to achieve the best SPR performance, i.e., sensitivity and FOM with the resonant reflectance close to 0, at a fixed probing wavelength. The simulated SPR curves are plotted in the function of Al film thickness for gas (Figure 4a) and aqueous (Figure 4b) medium. Al films from HH and LH conditions exhibit similar SPR curves and resonance angle shifts corresponding to the bulk refractive index change. We expect this since Al films from these two conditions have close values of n and k at 405 nm. Sensitivity, FOM, and resonant reflectance are determined to obtain the optimum thickness of Al films for gas and aqueous solution sensing, respectively (Figure 4 bottom row).

For gas sensing, the sensitivity is almost constant among Al films with different thicknesses from the same deposition condition. FOM is also constant for HH and LH conditions. For the LL condition, the FOM decreases as the Al film thickness increases. Based on this simulation result, we should select Al films having the minimum resonant reflectance for practical applications. Al films from the three deposition conditions have the same sensitivity 65°/RIU with the lowest resonant reflectance (16 nm for HH and LH conditions and 19 nm for the LL condition). For aqueous solution sensing, we observe similar features in that the sensitivity is almost constant among different Al films from the HH and LH deposition conditions. A transparent green bar labels the Al thin films with resonant reflectance smaller than 0.01 for each deposition condition. For HH condition, these three Al films are 19, 20, and 21 nm thick with sensitivity 135, 140, and 135°/RIU, respectively. For LH condition, these three Al films are 18, 19, and 20 nm thick with sensitivity 130, and 135, and 135°/RIU, respectively. For LL condition, these three Al films are 20, 21, and 22 nm thick with sensitivity 150, 150, and 160°/RIU, respectively. The FOM increases first and then decreases as the Al film thickness increases for all three deposition conditions. Although the sensitivity of Al films from the LL condition increases as the thickness of the film increases, the resonant reflectance also increases. Considering the Al films from the LL condition have relatively rough surfaces that reduce the propagation lengths of the surface polaritons (SPs), we select the one (19 nm Al + 3 nm Al_2O_3, highlighted in Figure 3) from the HH condition for the experimental Al SPR sensing. We also compared our simulation results to the Rakic's Al SPR performance at 405 nm. The optimized thicknesses are 18 and 19 nm with sensitivity 130°/RIU for both films.

Experimental Measurement of Al SPR Sensitivity. We measured the SPR curve for each salt solution. Peak find function in Origin is used to fit the resonance angle of the measured angular reflectance curve with a dark dip (Figure 5a). The experimental SPR resonance angle matches the simulation result for each salt solution (Figure 5b). In the simulation, the refractive indices are set as the measured values for the cover medium (NaCl solution) and the selected Al film. The linear transduction region from 1.3311 to 1.3627 with the R-square 0.99964 is determined based on simulation results. The theoretical sensitivity is 146.2°/RIU, and the experimental result is 149.9°/RIU. The theoretical sensitivity of this 19 nm Al film is slightly different from the simulated value as shown in Figure 4b (135°/RIU), since the measured n and k of this specific film are varied from the average value. We compared our Al SPR sensor to those of other reported Al SPR sensors (Table 1). To our knowledge, this Al SPR sensor has the highest experimental sensitivity.

Surface Sensing. We incubated cytochrome-c protein on the surface of the Al film by injecting the protein solution into

https://doi.org/10.1021/acsomega.3c06855
ACS Omega 2023, 8, 43188−43196

Table 1. SPR Bulk Refractive Index Sensing Capability Comparison

Al + Al_2O_3 thickness	probing wavelength	experimental sensitivity
~23 nm[16]	266 nm	100°/RIU (calculated)
12 nm + 3 nm	650 nm	59.25°/RIU
20 nm[18]	507 nm	118.6°/RIU
19 nm + 3 nm [this work]	405 nm	149.9°/RIU

the flow cell. The SPR resonance angle increases after cytochrome-c protein solution injection (Figure 6a), and the FWHM of the SPR curve becomes broad (Figure 6b) due to the high optical absorptivity of this protein at 405 nm wavelength.[26] The SPR resonance angle decreases, and the FWHM becomes narrower during the stabilization process. The surface coverage of cytochrome-c reaches the maximum at the instance after the protein solution contacts the Al surface, and then, the surface coverage becomes lower as time passes by. Based on the exponential decay fitting (Figure 6a), the equilibrium surface coverage has an SPR resonance angle of 73.01° which is 0.04° higher compared to the buffer solution (72.97°, Al SPR: 1.33468, Abbe: 1.33433). We simulate the scenario of a single layer with complete coverage of cytochrome-c, and the resonance angle is 73.61°. The protein is 3.4 nm (free form in an aqueous environment), and the refractive index is 1.4 in the simulation model.[27] Even instantaneously after the injection, a full monolayer of cytochrome-c protein does not form on the Al surface. A similar phenomenon has been reported by others.[17] The surface hydrophilic property is measured (Figure 6c). Al films are more hydrophilic from the LL condition. We contribute this to the relatively rough surface of Al films from the LL condition.

DISCUSSION

Deposition Condition. A few research works have demonstrated that the experimental optical properties of Al films are not consistent with the theoretical calculation and varied among deposition techniques and conditions.[23,28] It is common that simulation and experimental results are inconsistent for metallic nano-optical devices. Our work proves that the deposition rate is more influential to Al films for SPR applications. Using the high deposition rate (150 A heating current, 1.47−3.41 nm/s) defined in our work, the Al films from the high (1×10^{-4} Pa approximate 7.50×10^{-7} Torr) and low vacuum (7×10^{-4} Pa approximate 5.25×10^{-6} Torr) levels have close optical property and both support SPR at 405 nm. It needs 8 h and 40 min to reach the defined high and low vacuum levels, respectively. There is no need to examine a higher or lower vacuum deposition condition. A low vacuum condition is sufficient for high-quality Al films as long as the high deposition rate is guaranteed and reaction with the residue gas in the chamber is avoided. Using the defined high deposition rate, at least 4.4 times slower deposition rate compared to the reported study (15 nm/s),[23] we have achieved Rakic like Al films.[24] The low deposition rate is constant as 0.1 nm/s at 120 A heating current. With the high deposition rate we used, a 23 nm thick Al film needs approximately 13.5 s, and this is a controllable process. This is critical for Al SPR sensors since the optimized thickness of these films is in the range from 16 to 21 nm based on our simulation results. If thinner Al films are requested, middle deposition rates should be used to extend the deposition time and the optical property of the resulted Al films should be examined. Based on our experimental results, the surface roughness (largest RMS 1.514 nm) of the deposited Al films is tiny, and SPR performance is not influenced. But to our observation, this relatively large surface roughness is highly influential in the Al thin film etching process for nanostructure metasurfaces, i.e., focused ion beam etching in our another research. The rough surface alters the ion beam focusing during the etching process, and the resulting patterns are out of shape compared to the designs.

Bulk Refractive Index Sensing. For bulk refractive index sensing, the propagation SPR using metallic thin films is not inferior to LSPR based on metallic nanostructures. Propagation SPR supports large sensing volumes. LSPR phenomenon is more suitable for nonlinear light−matter interaction-based transduction strategies to sense minute substances through the generated optical signal with different frequencies. LSPR provides a highly confined near-field with extremely high local intensity that is favorable to nonlinear processes. Al nanostructures have been applied in fundamental research,[29−33] polarization generation,[34] modifying light phase and intensity in the visible range,[35] color generation,[36−38] enhancing specific light−matter interactions,[39−42] biosens-

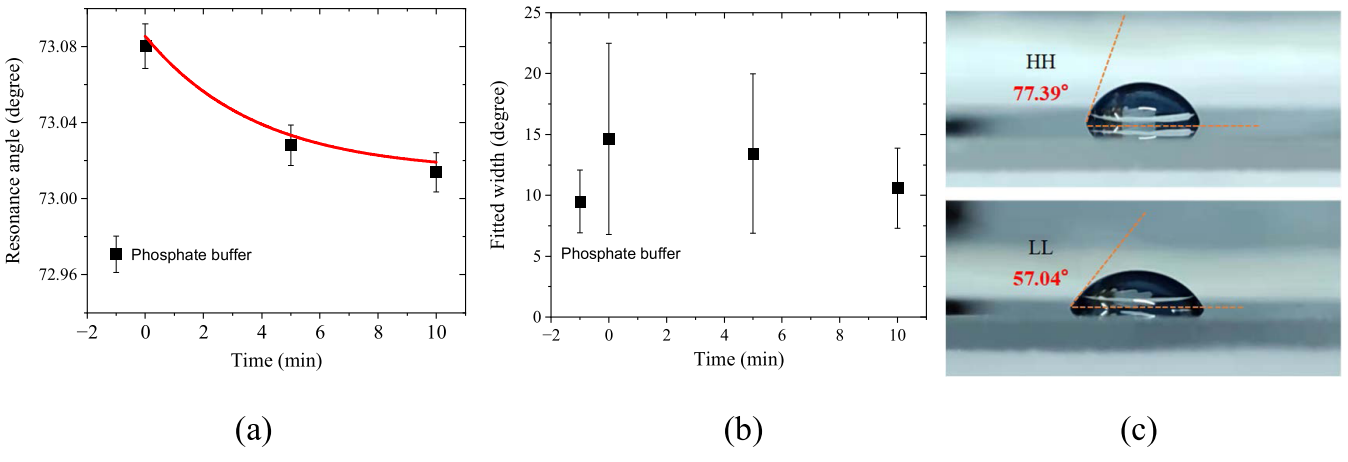

Figure 6. (a) Resonance angle and (b) FWHM of SPR curves before and after cytochrome-c protein solution injection. (c) Hydrophilic measurements of Al thin films from the HH and the LL deposition conditions.

https://doi.org/10.1021/acsomega.3c06855
ACS Omega 2023, 8, 43188−43196

ing,[43] nonlinear optics,[44,45] and others.[46−48] The strong localized near-field can cause photon damage to the sensing analytes, especially for biological samples. Optical absorption from the metallic materials generates a local thermal spike that can cause thermal shock to the sensing analytes or melt the nanostructures. Based on our experimental observation, as low as 3 μW incident power is enough for the Al SPR sensor using 405 nm light. Compared to Au SPR (~50°/RIU for gas and ~75°/RIU for aqueous solution as shown in Figure 2b of ref 49.), Al SPR at 405 nm has higher sensitivities (65°/RIU for gas and 140°/RIU for aqueous solution) based on our simulation works. Regarding the SPR and LSPR sensor designs, we suggest using the measured values of n and k for the Al material in the simulation models. The optical properties of Al films differ dramatically among different deposition techniques and conditions. Despite using the same technique and deposition parameters, the resulted Al thin films vary in properties due to the specific machine or person. Here, we emphasize that for a specific metallic film and a specific SPR probing wavelength, the thickness of the film should be optimized to reach the most sensitive performance.

Surface Sensing. For sensing analytes with strong light absorption, the angular interrogation is more proper. The broadened SPR curves due to the strong absorption make intensity interrogation with a fixed incident angle and probing wavelength impossible. Regarding the phase interrogation, the difficulty in the experimental setup hinders this strategy from being applied to SPR sensing techniques. Regarding the wavelength interrogation, complex refractive indices of all of the materials involved in the SPR excitation components should use wavelength-dependent values to obtain the information on the surface adsorbed analytes. The chemical configurations of the study analytes, especially biomolecules, e.g., proteins, antigens, and antibodies, can change due to the surface chemistry of the SPR sensors. Wavelength interrogation can be a possible way to measure the refractive index changes during the incubation process.

Angular Interrogation System. The trend of SPR sensing systems moves toward a low cost and broad working frequency range. Cheap light source is another factor to reduce the cost.[50] Our research shows that a simple LD excites the SPR phenomenon of Al thin films well. For the single incident angle interrogation strategy, the mechanical stability and angular resolution of the rotation stage are critical to the sensing capability. The intensity of the incident beam should be stable during the entire sensing process. The fluctuation in the light intensity may result in a false resonance angle. For the multiplexed angle interrogation strategy, the stationary system improves the mechanical stability of the whole setup. There is no need to use a high-angle-resolution rotation stage. The requirement shifts to the focusing lens on the incident light path, the collimating lens on the reflection light path, and the imaging camera. The ratio of pixel/angle determines the angular resolution, which is compromised to the range of incident angles. A spatial filter can improve the quality of the incident beam of our homemade system. Yet, this simple homemade system is sufficient. The background and the reference images are not mandatory with the multiplexed angle setup since we selected Al films having a resonance reflectance close to 0. The theoretical highest limit of detection (LOD) is 3.7×10^{-5} RIU of the current system assuming that 1-pixel resonance shift is detectable.

CONCLUSIONS

We achieved high sensitivity Al SPR sensors in the blue visible region. The simple thermal evaporation deposition with a relative low vacuum level (7×10^{-4} Pa) and slow deposition rate (150 A heating current, 1.47−3.41 nm/s) resulted in thin Al films with atomic surface roughness. The resulting Al films have refractive indices close to Rakic's. The sensitivity obtained for the aqueous bulk refractive index sensing is as high as 149.9°/RIU for the first time. So far, Al SPR sensors working in the deep UV, UV,[16] blue visible (this work), red visible,[17] and near-infrared regimes[18] have all been reported. Al material will boost the development of low cost, broad working frequency range, and COMS process compatible SPR sensors. The Al SPR sensor is possible to replace the standard Au SPR sensor in the near future.

ASSOCIATED CONTENT

Supporting Information

The Supporting Information is available free of charge at https://pubs.acs.org/doi/10.1021/acsomega.3c06855.

Details of the deposition procedure; ellipsometry fitting results of alumina thickness from 1 to 4 nm; comparison of Al optical properties among ref 23, Rakic's, and our work (PDF)

AUTHOR INFORMATION

Corresponding Author

Xue Han − *School of Optoelectrical Engineering and Instrumentation Science, Dalian University of Technology, Dalian 116024, China;* orcid.org/0000-0001-9525-1176; Email: xue_han@dlut.edu.cn

Authors

Chengchao He − *School of Optoelectrical Engineering and Instrumentation Science, Dalian University of Technology, Dalian 116024, China*

Yanhong Li − *School of Optoelectrical Engineering and Instrumentation Science, Dalian University of Technology, Dalian 116024, China*

Yuxiang Yang − *School of Optoelectrical Engineering and Instrumentation Science, Dalian University of Technology, Dalian 116024, China*

Huaikun Fan − *School of Optoelectrical Engineering and Instrumentation Science, Dalian University of Technology, Dalian 116024, China*

Dawei Li − *School of Optoelectrical Engineering and Instrumentation Science, Dalian University of Technology, Dalian 116024, China;* orcid.org/0000-0001-6967-4968

Complete contact information is available at: https://pubs.acs.org/10.1021/acsomega.3c06855

Author Contributions

†C.H. and Y.L. contributed equally to this work.

Notes

The authors declare no competing financial interest.

ACKNOWLEDGMENTS

The authors acknowledge the financial support from the National Natural Science Foundation of China (Grant Nos. 62105053 and 12274051) and the Fundamental Research

Funds for the Central Universities (Grant No. DUT21RC(3) 032).

REFERENCES

(1) Nylander, C.; Liedberg, B.; Lind, T. Gas detection by means of surface plasmon resonance. *Sens. Actuators* **1983**, *3*, 79−88.
(2) Huo, Z.; Li, Y.; Chen, B.; et al. Recent advances in surface plasmon resonance imaging and biological applications. *Talanta* **2023**, *255*, No. 124213.
(3) Qu, J. H.; Dillen, A.; Saeys, W.; et al. Advancements in SPR biosensing technology: An overview of recent trends in smart layers design, multiplexing concepts, continuous monitoring and in vivo sensing. *Anal. Chim. Acta* **2020**, *1104*, 10−27.
(4) Masson, J. F. Surface Plasmon Resonance Clinical Biosensors for Medical Diagnostics. *ACS Sens.* **2017**, *2* (1), 16−30.
(5) Menon, P. S.; Said, F. A.; Mei, G. S.; et al. Urea and creatinine detection on nano-laminated gold thin film using Kretschmann-based surface plasmon resonance biosensor. *PLoS One* **2018**, *13* (7), No. e0201228.
(6) Liu, X.; Huang, R.; Su, R.; et al. Grafting hyaluronic acid onto gold surface to achieve low protein fouling in surface plasmon resonance biosensors. *ACS Appl. Mater. Interfaces* **2014**, *6* (15), 13034−13042.
(7) Liu, H.; Wang, B.; Leong, E. S. P.; et al. Enhanced surface plasmon resonance on a smooth silver film with a seed growth layer. *ACS Nano* **2010**, *4* (6), 3139−3146.
(8) West, P. R.; Ishii, S.; Naik, G.; et al. Searching for better plasmonic materials. *Laser Photonics Rev.* **2010**, *4* (6), 795−808.
(9) Moreira, C.; Wang, Y.; Blair, S.; et al. Approaches for deep-ultraviolet surface plasmon resonance sensors. *Opt. Lett.* **2020**, *45* (16), 4642−4645.
(10) Ross, M. B.; Schatz, G. C. Aluminum and Indium Plasmonic Nanoantennas in the Ultraviolet. *J. Phys. Chem. C* **2014**, *118* (23), 12506−12514.
(11) Clark, B. D.; Lou, M.; Nordlander, P.; et al. Aluminum Nanocrystals Grow into Distinct Branched Aluminum Nanowire Morphologies. *Nano Lett.* **2020**, *20*, 6644−6650, DOI: 10.1021/acs.nanolett.0c02466.
(12) Jacobson, C. R.; Solti, D.; Renard, D.; et al. Shining Light on Aluminum Nanoparticle Synthesis. *Acc. Chem. Res.* **2020**, *53*, 2020−2030, DOI: 10.1021/acs.accounts.0c00419.
(13) Zorić, I.; Zäch, M.; Kasemo, B.; et al. Gold, platinum, and aluminum nanodisk plasmons: material independence, subradiance, and damping mechanisms. *ACS Nano* **2011**, *5* (4), 2535−2546.
(14) Zhu, X.; Imran Hossain, G. M.; George, M.; et al. Beyond Noble Metals: High Q-Factor Aluminum Nanoplasmonics. *ACS Photonics* **2020**, *7* (2), 416−424.
(15) Kochergin, V.; Neely, L.; Jao, C. Y.; et al. Aluminum plasmonic nanostructures for improved absorption in organic photovoltaic devices. *Appl. Phys. Lett.* **2011**, *98* (13), No. 133305.
(16) Tanabe, I.; Tanaka, Y. Y.; Ryoki, T.; et al. Direct optical measurements of far- and deep-ultraviolet surface plasmon resonance with different refractive indices. *Opt. Express* **2016**, *24* (19), 21886−21896.
(17) Lambert, A. S.; Valiulis, S. N.; Malinick, A. S.; et al. Plasmonic Biosensing with Aluminum Thin Films under the Kretschmann Configuration. *Anal. Chem.* **2020**, *92* (13), 8654−8659.
(18) Oliveira, L. C.; Herbster, A.; da Silva Moreira, C.; et al. Surface Plasmon Resonance Sensing Characteristics of Thin Aluminum Films in Aqueous Solution. *IEEE Sens. J.* **2017**, *17* (19), 6258−6267.
(19) Mroczyński, R.; Iwanicki, D.; Fetliński, B.; et al. Optimization of Ultra-Thin Pulsed-DC Magnetron Sputtered Aluminum Films for the Technology of Hyperbolic Metamaterials. *Crystals* **2020**, *10* (5), 384.
(20) Cheng, C.-W.; Liao, Y. J.; Liu, C. Y.; et al. Epitaxial Aluminum-on-Sapphire Films as a Plasmonic Material Platform for Ultraviolet and Full Visible Spectral Regions. *ACS Photonics* **2018**, *5* (7), 2624−2630.
(21) Cheng, F.; Su, P. H.; Choi, J.; et al. Epitaxial Growth of Atomically Smooth Aluminum on Silicon and Its Intrinsic Optical Properties. *ACS Nano* **2016**, *10* (11), 9852−9860.
(22) Knight, M. W.; King, N. S.; Liu, L.; et al. Aluminum for plasmonics. *ACS Nano* **2014**, *8* (1), 834−840.
(23) McPeak, K. M.; Jayanti, S. V.; Kress, S. J. P.; et al. Plasmonic Films Can Easily Be Better: Rules and Recipes. *ACS Photonics* **2015**, *2* (3), 326−333.
(24) Rakić, A. D. Algorithm for the Determination of Intrinsic Optical-Constants of Metal-Films—Application to Aluminum. *Appl. Opt.* **1995**, *34* (22), 4755−4767.
(25) Li, X.; Liu, L.; Zhao, J.; et al. Optical Properties of Sodium Chloride Solution Within the Spectral Range from 300 to 2500 nm at Room Temperature. *Appl. Spectrosc.* **2015**, *69* (5), 635−640.
(26) Collinson, M.; Bowden, E. F. UV-Visible Spectroscopy of Adsorbed Cytochrome c on Tin oxide electrode. *Anal. Chem.* **1992**, *64* (13), 1470−1476.
(27) Runge, A. F.; Rasmussen, N. C.; Saavedra, S. S.; et al. Determination of anisotropic optical constants and surface coverage of molecular films using polarized visible ATR spectroscopy. Application to adsorbed cytochrome c films. *J. Phys. Chem. B* **2005**, *109* (1), 424−431.
(28) Ekinci, Y.; Solak, H. H.; Löffler, J. F. Plasmon resonances of aluminum nanoparticles and nanorods. *J. Appl. Phys.* **2008**, *104* (8), No. 083107.
(29) Bisio, F.; Proietti Zaccaria, R.; Moroni, R.; et al. Pushing the high-energy limit of plasmonics. *ACS Nano* **2014**, *8* (9), 9239−9247.
(30) Dhindsa, P.; Solti, D.; Jacobson, C. R.; et al. Facet Tunability of Aluminum Nanocrystals. *Nano Lett.* **2022**, *22*, 10088−10094, DOI: 10.1021/acs.nanolett.2c03859.
(31) Garoli, D.; Schirato, A.; Giovannini, G.; et al. Galvanic Replacement Reaction as a Route to Prepare Nanoporous Aluminum for UV Plasmonics. *Nanomaterials* **2020**, *10* (1), 102.
(32) Martin, J.; Kociak, M.; Mahfoud, Z.; et al. High-resolution imaging and spectroscopy of multipolar plasmonic resonances in aluminum nanoantennas. *Nano Lett.* **2014**, *14* (10), 5517−5523.
(33) Li, R.; Wang, D.; Guan, J.; et al. Plasmon nanolasing with aluminum nanoparticle arrays. *J. Opt. Soc. Am. B* **2019**, *36* (7), E104−E111, DOI: 10.1364/JOSAB.36.00E104.
(34) Wu, P. C.; Tsai, W. Y.; Chen, W. T.; et al. Versatile Polarization Generation with an Aluminum Plasmonic Metasurface. *Nano Lett.* **2017**, *17* (1), 445−452.
(35) Zhang, Y.; Yang, X.; Gao, J. Twisting phase and intensity of light with plasmonic metasurfaces. *Sci. Rep.* **2018**, *8* (1), No. 4884.
(36) Lochbihler, H.; Kleemann, B. H. Semi-permeable resonant aluminum gratings for structural coloration in transmission. *Opt. Lett.* **2021**, *46* (9), 2200−2203.
(37) Zhang, F.; Martin, J.; Murai, S.; et al. Broadband scattering by an aluminum nanoparticle array as a white pixel in commercial color printing applications. *Opt. Express* **2020**, *28* (18), 25989.
(38) Miyata, M.; Hatada, H.; Takahara, J. Full-Color Subwavelength Printing with Gap-Plasmonic Optical Antennas. *Nano Lett.* **2016**, *16* (5), 3166−3172.
(39) Jiao, X.; Peterson, E. M.; Harris, J. M.; et al. UV Fluorescence Lifetime Modification by Aluminum Nanoapertures. *ACS Photonics* **2014**, *1* (12), 1270−1277.
(40) Sharma, B.; Cardinal, M. F.; Ross, M. B.; et al. Aluminum Film-Over-Nanosphere Substrates for Deep-UV Surface-Enhanced Resonance Raman Spectroscopy. *Nano Lett.* **2016**, *16* (12), 7968−7973.
(41) Cerjan, B.; Yang, X.; Nordlander, P.; et al. Asymmetric Aluminum Antennas for Self-Calibrating Surface-Enhanced Infrared Absorption Spectroscopy. *ACS Photonics* **2016**, *3* (3), 354−360.
(42) Pierce, D. R.; Bobbin, M.; Geddes, C. D. Fluorophore-Induced Plasmonic Current Generation from Aluminum Nanoparticle Films. *J. Phys. Chem. C* **2023**, *127* (2), 1126−1134.
(43) Li, W.; Ren, K.; Zhou, J. Aluminum-based localized surface plasmon resonance for biosensing. *TrAC, Trends Anal. Chem.* **2016**, *80*, 486−494.

https://doi.org/10.1021/acsomega.3c06855
ACS Omega 2023, 8, 43188−43196

(44) Yang, K. Y.; Butet, J.; Yan, C.; et al. Enhancement Mechanisms of the Second Harmonic Generation from Double Resonant Aluminum Nanostructures. *ACS Photonics* **2017**, *4* (6), 1522−1530.
(45) Stolt, T.; Vesala, A.; Rekola, H.; et al. Multiply-resonant second-harmonic generation using surface lattice resonances in aluminum metasurfaces. *Opt. Express* **2022**, *30* (3), 3620−3631.
(46) Lou, M.; Bayles, A.; Everitt, H. O.; et al. Selective Photodetoxification of a Sulfur Mustard Simulant Using Plasmonic Aluminum Nanoparticles. *Nano Lett.* **2022**, *22*, 7699−7705, DOI: 10.1021/acs.nanolett.2c03188.
(47) Morisawa, H.; Ono, A.; Inami, W.; et al. Hot-electron emission enhancement by deep UV surface plasmon resonance on an aluminum periodic disk-hole array. *Opt. Mater. Express* **2021**, *11* (7), 2278−2287, DOI: 10.1364/OME.428387.
(48) Honda, M.; Kumamoto, Y.; Taguchi, A.; et al. Efficient UV photocatalysis assisted by densely distributed aluminum nanoparticles. *J. Phys. D: Appl. Phys.* **2015**, *48* (18), No. 184006.
(49) Hassani, H.; Wolf, N. R.; Yuan, X.; et al. Platinum substrate for surface plasmon microscopy at small angles. *Opt. Lett.* **2020**, *45* (12), 3292−3295, DOI: 10.1364/OL.396051.
(50) Prabowo, B. A.; Purwidyantri, A.; Liu, K. C. Surface Plasmon Resonance Optical Sensor: A Review on Light Source Technology. *Biosensors* **2018**, *8* (3), No. 80, DOI: 10.3390/bios8030080.

https://doi.org/10.1021/acsomega.3c06855
ACS Omega 2023, 8, 43188−43196